Article

Ermeloite, $AlPO_4 \cdot H_2O$ a new phosphate mineral with kieserite-type structure from Galicia, Spain

Guillermo Z. Vérez[1]*, Carlos J. Rodríguez Vázquez[1], Bruno Dacuña Mariño[1], Inés Fernández Cereijo[1], José González del Tánago[2], Ramón Jiménez Martínez[3], Ramiro Barreiro Pérez[1], Raquel Antón Segurado[1], Ezequiel Vázquez Fernández[1], Montse Gómez Dopazo[1], Aida González Pazos[1] and Oscar Lantes-Suárez[1].

[1]Área de Infraestruturas de Investigación, Universidade de Santiago de Compostela. 15782 Galicia, Spain.

[2] Departamento de Mineralogía y Petrología, Facultad de Ciencias Geológicas, Universidad Complutense, 28040 Madrid, Spain.

[3] Departamento de Recursos Geológicos para la Transición Ecológica, Instituto Geológico y Minero de España (CSIC), 28003 Madrid, Spain.

*Author for correspondence: Guillermo Z. Vérez, E-mail: g.zaragoza@usc.es

Manuscript submission date: 02/11/2023

DOI: 10.1180/mgm.2024.33

Abstract

Ermeloite is a new aluminium phosphate mineral from Galicia (Spain), in the northwest of the Iberian Peninsula. It is the third formally recognized mineral discovered in Galicia since morenosite and cervantite in the 19th century. The name and symbol (Erm) were approved by the International Mineralogical Association (IMA2021-017a) in recognition of the geographical location where it was found. The mineral occurs as a light blue to white fine aggregate over quartz and microcline associated with wardite. Crystals of about 0.04 mm are transparent and have a waxy lustre. The simplified empirical formula determined using EPMA chemical analysis is $Al_{1.02}P_{0.95}F_{0.06}O_{3.88}\cdot 1.06\ H_2O$, which is near to the ideal formula $Al(PO_4)\cdot H_2O$. The mineral is an alteration product within a phosphate pegmatite. Ermeloite is the second phosphate isostructural with the sulphates of the kieserite group. Single crystal diffraction showed that ermeloite crystallises in the monoclinic *C*2/*c* space group with cell parameters a = 6.5371(4) Å, b = 7.5670(5) Å, c = 7.1146(5) Å; β = 115.335(2)°,V = 318.08(4) Å^3, Z=4 at room temperature. Comparative analysis of the crystallographic data, with isostructural phosphates, revealed an interesting behaviour for these compounds.

Keywords: Ermeloite, aluminum phosphate, new mineral, crystal structure, X-ray diffraction, Raman spectroscopy, electron microprobe analysis, pegmatite paragenesis

https://doi.org/10.1180/mgm.2024.33 Published online by Cambridge University Press

Introduction

At present, only two minerals whose type locality is in Galicia (Spain) are recognised by the IMA as unquestionable minerals. These minerals are morenosite from Cabo Ortegal, A Coruña (Martínez Alcíbar, 1850, 1851) and cervantite from Cervantes, Lugo (Dufrénoy, 1845). Therefore, ermeloite (Erm) is of great historical and social relevance as it is the first well-characterised mineral discovered in Galicia for more than 150 years. Furthermore, our understanding of the isostructural kieserite group is enhanced by the discovery of ermeloite.

The new mineral was found in a pegmatite outcropping in granodiorites of the Morrazo peninsula (Moaña, Pontevedra, Galicia, Spain). It was found in the southern part of a place known as "As Chans de Ermelo" (42°17'47"N, 8°45'12"W, ETRS89). The mineral and the name ermeloite have been approved by the IMA Commission on New Minerals and Mineral Names (IMA-CNMMN number 2021-017a). The type specimen (CMG4083) is kept in the Museo de Historia Natural of the University of Santiago de Compostela as part of the Galician Mineral Collection. The test sample used in the EPMA (Nº 21610) is kept in the Museo Geominero (CN IGME-CSIC, Madrid, Spain).

Experimental Methods

Wavelength-dispersive electron microprobe analyses for ermeloite were obtained using

https://doi.org/10.1180/mgm.2024.33 Published online by Cambridge University Press

a Jeol JXA-8900 instrument at the Universidad Complutense (Madrid, Spain). Standard operating conditions were as follows: accelerating voltage 15 kV, intensity probe current 20 nA, peak counting time 10 s, background counting time 5 s, beam diameter 5 μm. The standards used were almandine (Fe Kα), microcline (K Kα) and fluorapatite (P Kα, F Kα) (Jarosevich *et al.*, 1980); albite (Al Kα) (McGuire *et al.*, 1992). The results were processed with an on-line ZAF programme. The elemental analyses expressed as element wt% are presented in Table S1.

The presence of lithium was excluded by optical inductively coupled plasma (ICP) using a PerkinElmer Optima 4300 DV ICP-OES spectrometer equipped with PerkinElmer AS-93plus autosampler. The sample was digested with HCl, HF and HNO_3 in a microwave reactor, for 45 minutes at 250 °C.

The Raman spectrum of emeloite was collected on a randomly oriented crystal using a WITec alpha300 R confocal Raman microscope operated with ultra-high throughput spectrometer (UHTS300), coupled by fibre to a 532 nm, 6.8 mW solid-state laser and a charge-coupled device (CCD) back-illuminated detector operating at –60 °C. A Zeiss EC Epiplan Neofluar 50x/0.8 objective was used. Automatic autofocus and a monochromator grating of 600 grooves/mm were used.

Powder X-ray diffraction patterns (PXRD) data were obtained using a Philips PW1710 powder diffractometer with a Philips PW1820/00 vertical goniometer and a FR590 Enraf Nonius X-ray generator. The instrument was equipped with a graphite-diffracted beam monochromator and copper radiation source (λ ($CuK\alpha_1$) = 1.5406 Å), operating at 40 kV and 30 mA. Diffraction data were collected using a scintillation counter for a range of 2–65° in 2Θ with a step size of 0.02° and counting time of 1 s/step. The powdered sample was spread over a low-background plate sample holder (Si 511) to minimize the background noise and the effect of preferred orientation. The sample was spun during the

https://doi.org/10.1180/mgm.2024.33 Published online by Cambridge University Press

data collection to improve the measurement statistics.

Unit cell parameters indexed by single crystal X-ray diffraction were refined using experimental data from a polycrystalline sample by the Pawley method using the HighScorePlus software (v. 3.0d (3.0.04), © PANalytical B. V.; Degen *et al.*, 2014). Peak assignments and intensities for the observed and calculated patterns are shown in Table 1, and a graphical interpretation in Fig. S1.

A light blue crystal suitable for single crystal diffraction (0.05 × 0.04 × 0.03 mm) was carefully selected, using cross-polarised light on an optical microscope with x90 magnification. The measurements were carried out at ambient temperature.

Single-crystal X-ray studies were performed on a Bruker D8 Venture Photon III-14 diffractometer using Incoatec multilayer mirror monochromated Mo-Kα radiation (λ = 0.71073 Å) from a microfocus sealed tube source at 298 K. Data for crystal structure determination were collected by omega and phi scans. Data reduction was performed using the APEX3 v2018.7-2 software package. An empirical absorption correction was applied using the SADABS 2016/2 program. The structure was solved using SHELXT 2018/2 (Sheldrick, 2015) and finally refined by full-matrix least-squares method based on F^2 by SHELXL2018/3 (Sheldrick, 2015). Neutral atom scattering curves were used. All non-hydrogen atoms were anisotropically refined. Hydrogen atom positions were included in the model based on Fourier difference electron density maps and refined without geometric constrains. Experimental details and cell parameters are given in Table 2. The bond valence analysis was performed using the latest values of the bond-valence parameters included in "bvparm2020.cif" data set from the IUCr, following the methodology of Witzke *et al.* (2000) and Brown (2006).

Occurrence

https://doi.org/10.1180/mgm.2024.33 Published online by Cambridge University Press

The intrusive suite of granodiorites of the Morrazo peninsula belongs to the Bayo-Vigo Massif. At the centre of this area is the Festiñazo granodiorite (Fig. 1), which presents potassium feldspar megacrystals (3-4 cm) inside a matrix of fine to medium-grained plagioclase, quartz, biotite and muscovite (Gallastegui Suárez, 2005). Within these granodiorites, decimetric to metric pegmatitic dykes occur, which are probably genetically associated to nearby two-mica granites (Rubio Navas, 1981; Gallastegui Suárez, 2005).

The pegmatite in which the ermeloite appears does not present miarolitic cavities or textural zonation. The main rock-forming minerals include quartz, microcline, albitic plagioclase, biotite, muscovite and occasionally some primary Fe/Mn phosphates. Hydrothermal alteration has produced secondary minerals with variable contents of (OH) and H_2O (heterosite, troleite, crandalite, fluorapatite, rockbridgeite-frondelite, jansite-(CaMnMn), wardite, burangaite, mitridatite, phosphosiderite-strengite and cacoxenite). The sample of ermeloite studied is an ovoid nodule measuring 17.5×11.1 mm, embedded in albitic plagioclase.

The mineral occurs as short-prismatic crystals with a maximum size of 0.05 mm (Fig. 2). The colour of the mineral ranges from light blue to white and the streak is white. The crystals have a vitreous to pearly lustre and are transparent in thin fragments. Ermeloite is brittle and shows a conchoidal fracture. Mohs hardness is 3.5-4. The calculated density is 2.923 g/cm3. No fluorescence was detected under ultraviolet light. Optical properties could not be measured due to the microgranular nature of the specimen (Fig. S2).

Results and discussion

Composition

The results of the electron microprobe analyses of ermeloite are presented in Table 3.

https://doi.org/10.1180/mgm.2024.33 Published online by Cambridge University Press

The empirical formula obtained from the chemical analysis is $Al_{1.022}Fe_{0.002}K_{0.003}P_{0.950}F_{0.055}H_{2.120}O_{4.950}$. The simplified formula is $Al_{1.02}P_{0.95}F_{0.06}O_{3.88}\cdot 1.06\ H_2O$ (elements present in amounts less than 0.01 *apfu* have not been included in the simplified formula). This simplified formula is close to the ideal formula $AlPO_4\cdot H_2O$. The water content has been calculated by difference, and it is in agreement with crystallographic data.

Raman spectroscopy

The Raman spectrum of ermeloite was recorded between 100 and 3700 cm^{-1} (Fig. 3). In the region above 1200 cm^{-1}, it shows a weak intensity band at 1542 cm^{-1}, trapezoidal bands in the 2100–2800 cm^{-1} region, and broad bands centred at 3150 and 2996, cm^{-1}. These bands were tentatively assigned on the basis of literature data for related compounds. For example, in Kieserite-type compounds, bands at 1500 cm^{-1} and 3100–3400 cm^{-1} are reported as ν_2 bending and ν_1, ν_3 stretching modes of H_2O (A. Wang *et al.*, 2006; D. Talla and M. Widner, 2019 or C. Chio 2007). Bands around 2800 cm^{-1} in the IR spectrum were assigned to ν(MnO–H) or $\nu(H_3O^+)$ in serrabrancaite (Aranda and Bruque, 1990) and (Boonchom *et al.*, 2008), but these Raman spectroscopy techniques are highly sensitive to organic impurities, which result in characteristic C–H bond vibrations in the 2800– 3000 cm^{-1} and 1400–1500 cm^{-1} regions, (A Redkov *et al* (2019) and references cited therein). Therefore, the assignment of these bands for the case of natural systems is a matter of debate in the specialized literature.

In the region below 1200 cm^{-1}, the Raman shift is in good agreement with spectral bands obtained by other authors (Breitinger *et al.*, 2004; Frost *et al.*, 2004, 2014) for different phosphate minerals such as variscite, phosphosiderite, or wardite. Three bands at 1126, 1080, and 1008 cm^{-1} are present in the Raman ν_1 symmetric and ν_3 antisymmetric

https://doi.org/10.1180/mgm.2024.33 Published online by Cambridge University Press

stretching region (900–1200 cm^{-1}) of PO_4^{3-}. Bands at 617, 514, and 427 cm^{-1} can be assigned to ν_4 out-of-plane and ν_2 in-plane bending modes of phosphates. Finally, the Raman spectrum of ermeloite in the 180–350 cm^{-1} region shows a strong intense band near 317 cm^{-1}, and two others at 257 and 187 cm^{-1}. Raman bands below 300 cm^{-1} reported in the literature are related to the O–M–O skeleton vibrational modes, such as the Al–O stretching mode at 326 cm^{-1} in variscite or metavariscite or the O–M–O symmetric bending mode of strengite at 193 cm^{-1} and variscite at 230 cm^{-1} (Frost *et al.*, 2014).

Crystal structure

Single crystal diffraction shows that ermeloite crystallises in the monoclinic space group *C*2/*c* with cell parameters *a* = 6.5371(4) Å, *b* = 7.5670(5) Å, *c* = 7.1146(5) Å; β = 115.335(2)°, *V* = 318.08(4) $Å^3$, *Z*=4. Atomic positions are given in Table 4.

Ermeloite presents a kieserite-type structure constructed of kinked chains of corner-sharing AlO_6 elongated octahedrons along [101], where the shared O3 oxygen atom is part of an H_2O molecule. These chains are further connected by regular PO_4 tetrahedra through the O2 oxygen atoms, forming chains described by (Moore, 1970) as '7 Å chains', (Fig. 4a). The tetrahedral vertices not directly linked to the central octahedral chain cross-link with adjacent chains, to form a mixed tetrahedral-octahedral framework through O1 atoms (Fig. 4b). These structural arrangements are stabilised by hydrogen bonds between O3 and adjacent O2 atoms along the *a* axis (Fig. 4d).

Bond distances and angles for octahedral and tetrahedral units are reported in Table 5. The average <P–O> bond lengths (1.5303 Å) and <O–P–O> angles (109.47°) indicate that the phosphate tetrahedron is quite regular, in good agreement with the value obtained by (Baur, 1974) (<P–O> = 1.537 Å) and confirmed by (Huminicki and Hawthorne, 2019) for minerals containing ($P\phi_4$) tetrahedra. The observed P–O2 distance (1.5454(14) Å) is

https://doi.org/10.1180/mgm.2024.33 Published online by Cambridge University Press

typical of a single P–O bond (1.546 Å), while the P–O1 distance (1.5152(14) Å) is significantly shorter than a single bond and slightly longer than a double P=O bond (1.504 Å), thereby indicating a delocalisation of the charge along O1–P–O1.

The aluminum atoms are [2+2+2] coordinated with four phosphates in an equatorial plane (through O1 and O2) and two H_2O molecules (O3) in axial positions (Fig. 4c). According to Schindler and Hawthorne (1999), the only way to stabilize [M^{3+} ($T^{5+}O_4$) (H_2O)] structures in the kieserite group arrangement, and for the M^{3+}–(O3)–M^{3+} linkage to occur require an elongation of the M^{3+}–O3 bonds to make the incident bond-valence sums around the bridging anion compatible. The Al^{3+} cation has a $3d^0$ electronic configuration, like Mg^{2+}, but the required elongation, is greater in trivalent compounds than in divalent ones, as is evidenced in figure S4. Mn^{3+} and V^{3+} present M-O3 bond lengths similar to bulkier M^{2+} cations, and at less 0.1A greater than would be expected for a divalent cation with the same ionic radius. This large elongation requirement makes it surprising that the $AlPO_4{\cdot}H_2O$ species crystallises in a Kieserite-type structure, as the cation lacks a specific electron mechanism to induce the required elongation.

The compatibility of this Al^{3+}–(O3)–Al^{3+} arrangement in the kieserite-type structure, with bond-valence sums in the ermeloite, can be observed in Table 6. The structure compensates for the deficiencies in the formal incident bond-valence sums mainly by shortening the bonds to O1 and lengthening those to O3. This can be observed in the largest Al–O3 distance (2.0509(9) Å) compared to Al–O2 (1.8662(13) Å), and Al–O1 (1.8158(13) Å). These values differ significantly from the Al–O bond distances recorded in the Cambridge database for AlO_6 (Fig. S3). The corresponding bond angles, O1–Al–O2, O1–Al–O3, and O2–Al–O3, are 87.13(6)°, 88.13(4)°, and 87.14 (6)°, respectively. These angles represent deviations of less than 2.9° from the ideal angles. Interestingly, the elongation of the Al–O3 bond occurs without significant alterations in the octahedral

https://doi.org/10.1180/mgm.2024.33 Published online by Cambridge University Press

angles. This phenomenon may be facilitated by the presence of a square-plane in the equatorial position, formed by four different phosphates (Fig. 4d), resulting in a relatively low-tension octahedral configuration, which is further evidenced by a high quadratic elongation value (1.008), despite the relatively low variance in octahedral angles (7.23 deg^2). Similar trends were also observed for other isostructural phosphates (Fig. S5). This behaviour differs from the general observations reported by (Robinson *et al.*, 1971) for different cations in different families of minerals, such as olivines, humites, garnets, amphiboles, pyroxenes, etc. For divalent kieserites (sulphates and selenates) an intrinsic value of the elongation is observed but, the octahedral distortion is lower than for phosphates (Fig. S5).

The corner-sharing octahedral chains have an angular relationship of 126.25(10)° between consecutive octahedrons (M–O3–M). In addition, they feature angles of 141.98(9)° and 131.30°(8) with respect to adjacent chains, as determined by the Al–O1–P and Al–O2–P angles, respectively. Finally, the refined bond distances O3-H 0.84(3)Å and the dihedral angle H-O3-H 104(4)° of the water molecule present appropriate values, and the strong hydrogen bonding interactions are evidenced by the short O3…O2 distance (2.6356(17) Å).

Relationship with isostructural phosphates

The new mineral ermeloite is isostructural with kieserite-type compounds of general stoichiometry $[M(TO_4)\cdot(H_2O)]$ (M = Mg^{2+}, Fe^{2+}, Ni^{2+}, Co^{2+}, Mn^{2+}, Zn^{2+}; T = S, Se) (Leonhardt and Weiss, 1957; Bregeault *et al.*, 1970, Wildner, M. and Giester, G. (1991)) and two other phosphates(M = Mn^{3+}, V^{3+}; T = P): serrabrancaite $MnPO_4\cdot H_2O$ (Lightfoot *et al.*, 1987; Witzke *et al.*, 2000) and synthetic $VPO_4\cdot H_2O$ (Vaughey *et al.*, 1994).

For better comparison with ermeloite, a unit cell transformation was performed to orient the structure like kieserite, with octahedral chains along [001] (Fig. S6). New

https://doi.org/10.1180/mgm.2024.33 Published online by Cambridge University Press

crystallographic settings (a′,b′,c′,β′) will be used, to refer to this new orientation.

Influence of the ionic radius of cations

The influence of the ionic radius of divalent cations on structural parameters (bond distances and angles) and cell dimensions (volume, axial lengths, or cell angles) has previously been analysed for kieserite group sulphates (T = S) (Hawthorne *et al.*, 1987; Wildner and Giester, 1991) and isostructural selenates (T = Se) (Giester and Wildner, 1992).These works provided evidence of a gradual variation in the crystallographic axes *a′* and *c′*, while the *b′* axis and the *β′* angle showed only minor deviations.

In the phosphates examined, notably distinct values were observed for the *b′* axis, together with significant variations in all the cell parameters in the case of serrabrancaite. However, when analysing Fig. 5a, 5b, in particular the cases of V^{3+} and Mn^{3+} (with similar ionic radius), the data suggest that all the variations in cell dimensions are produced so that the overall volume of the unit cell adapts to the ionic radius of the cation. Significant differences in the Mn–O bond distances were also observed in the case of serrabrancaite (Fig. 5d), possibly stemming from an increased M–O3 elongation due to the well-known Jahn-Teller effect (high-spin t_{2g}^3 e_g^1 configuration) in Mn^{3+} (Burns *et al.*, 1994), but overall, an increase in ionic radius leads to a linear rise in the average <M–O> bond lengths, in agreement with Kuppuraj *et al.* (2009). Consequently, this increase is reflected in the polyhedral volume, as depicted in Fig. 5c. The pronounced elongation of the O3 direction in phosphates is counterbalanced by a reduction in M–O2 and (especially) M–O1 distances to maintain an appropriate octahedral volume.

The P–O–M bond angles between adjacent chains range from 137° (M = V^{3+}) to 142° (M = Al^{3+}) for O1 and from 129° (M = V^{3+}) to 135° (M = Mn^{3+}) for O2. This implies greater variations in bond angles compared to sulphates and selenates, which show variations of about 1° for O1 and 3° for O2. Furthermore, these angles do not increase

https://doi.org/10.1180/mgm.2024.33 Published online by Cambridge University Press

smoothly with the size of the cation, as observed for divalent compounds, except for Mg^{2+} (Fig. 5e). In contrast, the M–O3–M angle decreases with the ionic radius of the cations, aligning with expected behaviour.

Relationship between cell axis lengths and geometric parameters

Factors that influence the length of cell parameters are difficult to identify in the case of the isostructural phosphates ermeloite, serrabrancaite, and synthetic $VPO_4 \cdot H_2O$, as only three compounds can be compared. Hence, definitive conclusions cannot be drawn. However, those that might have a logical relationship and a reasonable trend have been analysed. The main characteristic of these compounds is their long M–O3 bond. This elongation occurs along the *c′* axis. It is therefore reasonable to infer that the *c′* axis parameters observed in phosphates are associated with the significant elongation of the M–O3 bonds, as depicted in Fig. 6a. Similarly, the *a′* axis also appears to exhibit an almost linear behaviour with the elongation of M–O3 (Fig. 6b). This could be due to the relative positions of the phosphate anion and the H_2O molecule involved in the H-bonds between O3 and O2 along the *a′* axis. Finally, a reverse effect on the *b′* axis is observed with increasing M–O–P angle (Fig 6c). Giester and Wildner (1992) attributed differences in cell axis dimensions between sulphates and selenates to a variation in M–O–T angles caused by anion rotations around the *b′* axis. Interestingly, a linear relationship between these angular values is maintained in the three phosphates studied.

Conclusions

Ermeloite, a new phosphate mineral with the ideal formula $AlPO_4 \cdot H_2O$, has been discovered in Chans de Ermelo, Galicia, Spain. It is the third new mineral species discovered in Galicia. It is monoclinic and crystallises in the *C*2/*c* space group with cell parameters a = 6.5371(4) Å, b = 7.5670(5) Å, c = 7.1146(5) Å; β = 115.335(2)°, V =

https://doi.org/10.1180/mgm.2024.33 Published online by Cambridge University Press

318.08(4) Å^3, $Z = 4$. The mineral has a kieserite-type structure, showing that cations such as Al^{3+} with the formula [M^{3+} ($T^{5+}O_4$) (H_2O)] and without d orbitals or Jahn-Teller effect, can be present in members of this structural type.

Comparisons of crystallographic data show significant variations between serrabrancaite MnPO4·H2O and the isostructural phosphates ermeloite and $VPO_4·H_2O$. However linear relationships were observed for the two unit cell parameters (oriented as kieserite) *a′* and *c′* with M–O3 bond lengths, while *b′* showed an inverse linear relationship with increasing M–O–P angle. Unfortunately, with only three data points, these trends cannot be truly established.

Acknowledgements

The authors would like to thank Moisés Núñez and Manuel Cerviño for their contribution to this discovery and Dr. Antonio L. Llamas-Saiz and Prof Lionel Delaude revising the manuscript. This research was funded by the Área de Infraestruturas de Investigación of the Universidade de Santiago de Compostela (USC). All the analyses were carried out at the Área de Infraestructuras de Investigación (USC) except for the EPMA analysis, which was done with the assistance of Alfredo Fernández Larios, at the Centro de Microscopia Electrónica, Universidad Complutense (Madrid, Spain). We appreciate the efforts of the reviewers and editors to improve this article.

Competing interest

The authors declare none.

References

https://doi.org/10.1180/mgm.2024.33 Published online by Cambridge University Press

Aranda, M.A.G. and Bruque, S. (1990) Characterization of manganese(III) orthophosphate hydrate. *Inorganic Chemistry*, **29**, 1334–1337.

Baur, W.H. (1974) The geometry of polyhedral distortions. Predictive relationships for the phosphate group. *Acta Crystallographica Section B Structural Crystallography and Crystal Chemistry*, **30**, 1195–1215.

Boonchom, B., Youngme, S., Maensiri, S. and Danvirutai, C. (2008) Nanocrystalline serrabrancaite ($MnPO_4 \cdot H_2O$) prepared by a simple precipitation route at low temperature. *Journal of Alloys and Compounds*, **454**, 78–82.

Bregeault, J.M., Herpin, J.M., Manoli, J.M. and Pannetier, G. (1970) Affinement de la structure de la Kieserite $MgSO_4 \cdot H_2O$). *Bulletín de la Société Chimique de France*, **12**, 4243–4248.

Breitinger, D.K., Belz, H.-H., Hajba, L., Komlósi, V., Mink, J., Brehm, G., Colognesi, D., Parker, S.F. and Schwab, R.G. (2004) Combined vibrational spectra of natural wardite. *Journal of Molecular Structure*, **706**, 95–99.

Brown, I.D. (2006) *The Chemical Bond in Inorganic Chemistry: The Bond Valence Model*. *International Union of Crystallography Monographs on Crystallography*. Oxford University Press, Oxford, 292 pp.

Burns, P.C., Cooper, M.A. and Hawthorne, F.C. (1994) Jahn-Teller-distorted $Mn^{3+}O_6$ octahedra in fredrikssonite, the fourth polymorph of $Mg_2Mn^{3+}(BO_3)O_2$. *Canadian Mineralogist*, **32**, 397–403.

Degen, T., Sadki, M., Bron, E., König, U. and Nénert, G. (2014) The HighScore suite. *Powder Diffraction*, **29**, S13–S18.

Dufrénoy, A. (1845) *Traite de Minéralogie*. Carilian Goevry et Vr. Dalmont Editeurs, Paris, vol 2. 654-655 pp.

Frost, R.L., Weier, M.L., Erickson, K.L., Carmody, O. and Mills, S.J. (2004) Raman

https://doi.org/10.1180/mgm.2024.33 Published online by Cambridge University Press

spectroscopy of phosphates of the variscite mineral group. *Journal of Raman Spectroscopy*, **35**, 1047–1055.

Frost, R.L., Scholz, R., López, A., Lana, C. and Xi, Y. (2014) A Raman and infrared spectroscopic analysis of the phosphate mineral wardite $NaAl_3(PO_4)_2(OH)_4 \cdot 2(H_2O)$ from Brazil. *Spectrochimica Acta Part A: Molecular and Biomolecular Spectroscopy*, **126**, 164–169.

Gallastegui Suárez, G. (2005) Petrología del Macizo granodiorítico de Bayo – Vigo (Provincia de Pontevedra, España). Tesis Doctoral Universidad de Oviedo. *Laboratorio Xeolóxico de Laxe, Serie Nova Terra*, **26**, 414. Edicións do Castro, Sada. A Coruña.

Giester, G. and Wildner, M. (1992) The crystal structures of kieserite-type compounds. II. Crystal structures of $Me(II)SeO_4 \cdot H_2O$ (Me = Mg, Mn, Co, Ni, Zn). *Neues Jahrbuch für Mineralogie Monatshefte*, **3**, 135–144.

Hawthorne, F.C., Groat, L.A., Raudsepp, M. and Ercit, T.S. (1987) Kieserite , $MgSO_4 \cdot H_2O$, a titanite-group mineral. *Neues Jahrbuch für Mineralogie - Abhandlungen*, **157**, 121–132.

Huminicki, D.M.C. and Hawthorne, F.C. (2019) The crystal chemistry of the phosphate minerals. *Phosphates: Geochemical, Geobiological and Materials Importance*, **48**, 123–254.

Jarosevich, E., Nelen, J.A. and Norberg, J.A. (1980) Reference Samples for Electron Microprobe Analysis. *Geostandards and Geoanalytical Research*, **4**, 43–47.

Kuppuraj, G., Dudev, M. and Lim, C. (2009) Factors Governing Metal−Ligand Distances and Coordination Geometries of Metal Complexes. *The Journal of Physical Chemistry B*, **113**, 2952–2960.

Leonhardt, J. and Weiss, R. (1957) Das Kristallgitter des Kieserits $MgSO_4 \cdot H_2O$. *Die*

https://doi.org/10.1180/mgm.2024.33 Published online by Cambridge University Press

Naturwissenschaften, **44**, 338–339.

Lightfoot, P., Cheetham, A.K., Sleight, A.W., Tayal, V.P., Khandelwal, D.P., Bist, H.D., Redkov, A., Melehin, V., Zhurikhina, V., Frost, R.L., Weier, M.L., Erickson, K.L., Carmody, O., Mills, S.J., Petruševski, V.M., Aleksovska, S., Pluth, J.J. and Smith, J. V. (1987) Structure of $MnPO_4 \cdot H_2O$ by Synchrotron X-ray Powder Diffraction. *Inorganic Chemistry*, **26**, 3544–3547.

Martínez Alcíbar, A. (1850) Raro e importante mineral de níquel. *Revista Minera*, **1**, 302–306.

Martínez Alcíbar, A. (1851) Sobre el mineral de nickel de Galicia, con algunas consideraciones sobre el polimorfismo del sulfato de níquel y de otras sustancias. *Revista Minera*, **2**.

McGuire, A. V., Francis, C.A. and Dyar, M.D. (1992) Mineral standards for electron microprobe analysis of oxygen. *American Mineralogist*, **77**, 1087–1091.

Moore, P.B. (1970) Crystal chemistry of the basic iron phosphates. *American Mineralogist*, **55**, 135–169.

Robinson, K., Gibbs, G. V. and Ribbe, P.H. (1971) Quadratic elongation: A quantitative measure of distortion in coordination polyhedra. *Science (New York, N.Y.)*, **172**, 567–570.

Rubio Navas, J. (1981) *Memoria del Mapa Geológico de España a escala 1:50.000, Hoja 223 (Vigo)*. Madrid, 34 pp.

Schindler, M. and Hawthorne, F.C. (1999) Schubnelite, $[Fe^{3+}(V^{5+}O_4)(H_2O)]$, a novel heteropolyhedral framework mineral. *American Mineralogist*, **84**, 665–668.

Sheldrick, G.M. (2015) Crystal structure refinement with SHELXL. *Acta Crystallographica Section C Structural Chemistry*, **71**, 3–8. International Union of Crystallography.

https://doi.org/10.1180/mgm.2024.33 Published online by Cambridge University Press

Vaughey, J.T., Harrison, W.T.A., Jacobson, A.J., Goshorn, D.P. and Johnson, J.W. (1994) Synthesis, structure, and properties of two new vanadium(III) phosphates: $VPO_4 \cdot H_2O$ and $V_{1.23}(PO_4)(OH)_{0.69}(H_2O)_{0.31} \cdot 0{,}33\ H_2O$. *Inorg. Chem,* **33**, 2481–2487.

Wildner, M. and Giester, G. (1991) The crystal structures of kieserite-type compounds. I. Crystal structures of $Me(II)SO_4 \cdot H_2O$ (Me = Mn, Fe, Co, Ni, Zn). *Neues Jahrbuch für Mineralogie Monatshefte*, **7**, 296–306.

Witzke, T., Wegner, R., Doering, T., Pöllmann, H. and Schuckmann, W. (2000) Serrabrancaite, $MnPO_4 \cdot H_2O$, a new mineral from the Alto Serra Branca pegmatite, Pedra Lavrada, Paraiba, Brazil. *American Mineralogist*, **85**, 847–849.

List of figures

https://doi.org/10.1180/mgm.2024.33 Published online by Cambridge University Press

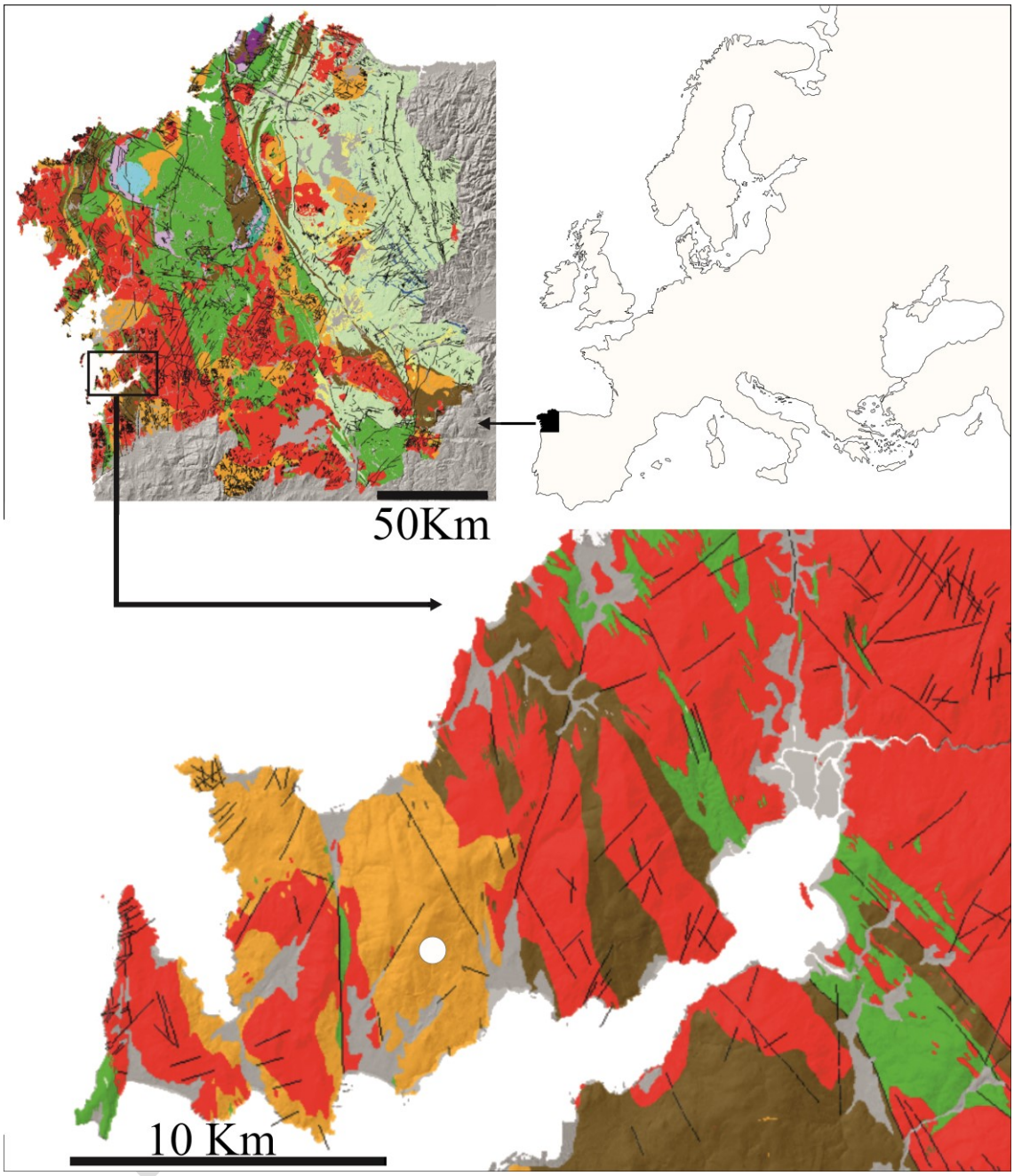

Fig. 1. Geographical location and geological context of ermeloite. Image top left: Galicia (black spot) in Europe. Image top right: Galicia and its geology. Image below: Zoom on the Morrazo peninsula and its geology. Orange: granodiorite with feldspar megacrystals (pegmatite with the ermeloite). Brown: biotitic gneiss. Green: micaschists and paragneiss with plagioclase and biotite. Pale green: schists and quartzites. Red: alkaline feldspar granite. Grey: quaternary deposits. White: Atlantic Ocean. White dot: ermeloite location.

https://doi.org/10.1180/mgm.2024.33 Published online by Cambridge University Press

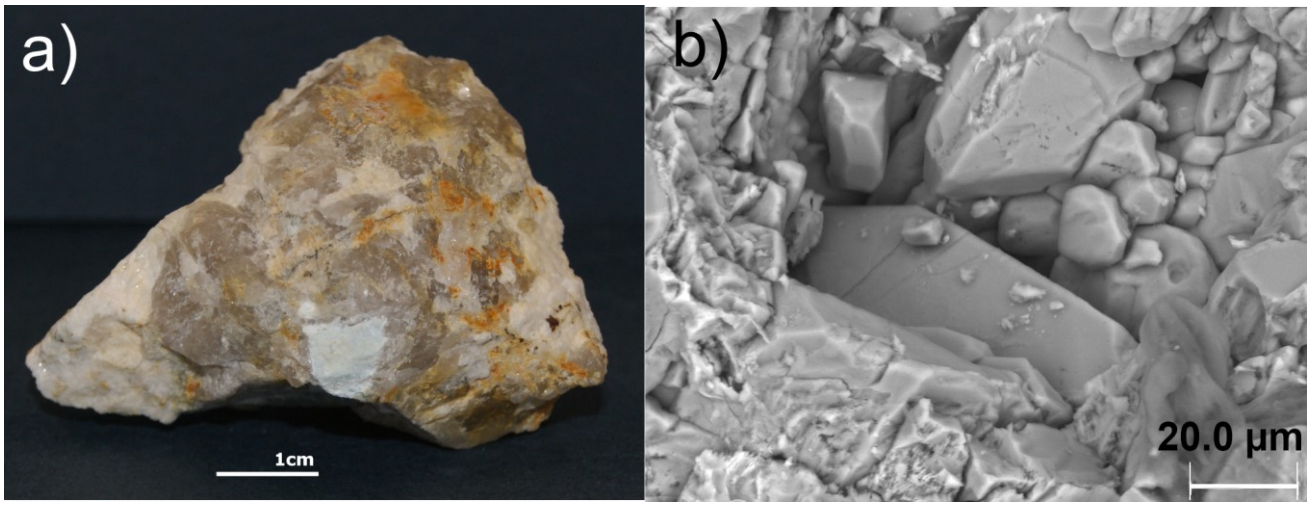

Fig. 2. a) Mineral photographs, b) SEM image of ermeloite crystalline mass.

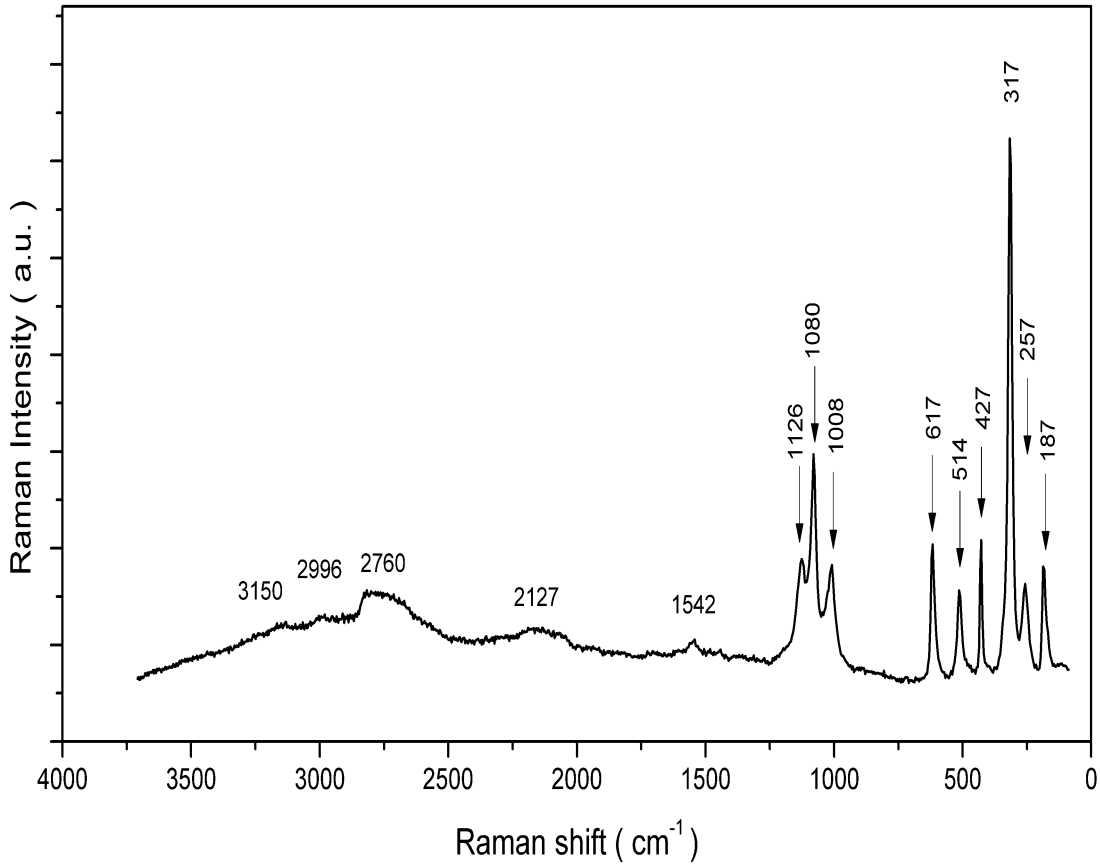

Fig. 3. Raman spectrum of ermeloite over randomly oriented crystal**.**

https://doi.org/10.1180/mgm.2024.33 Published online by Cambridge University Press

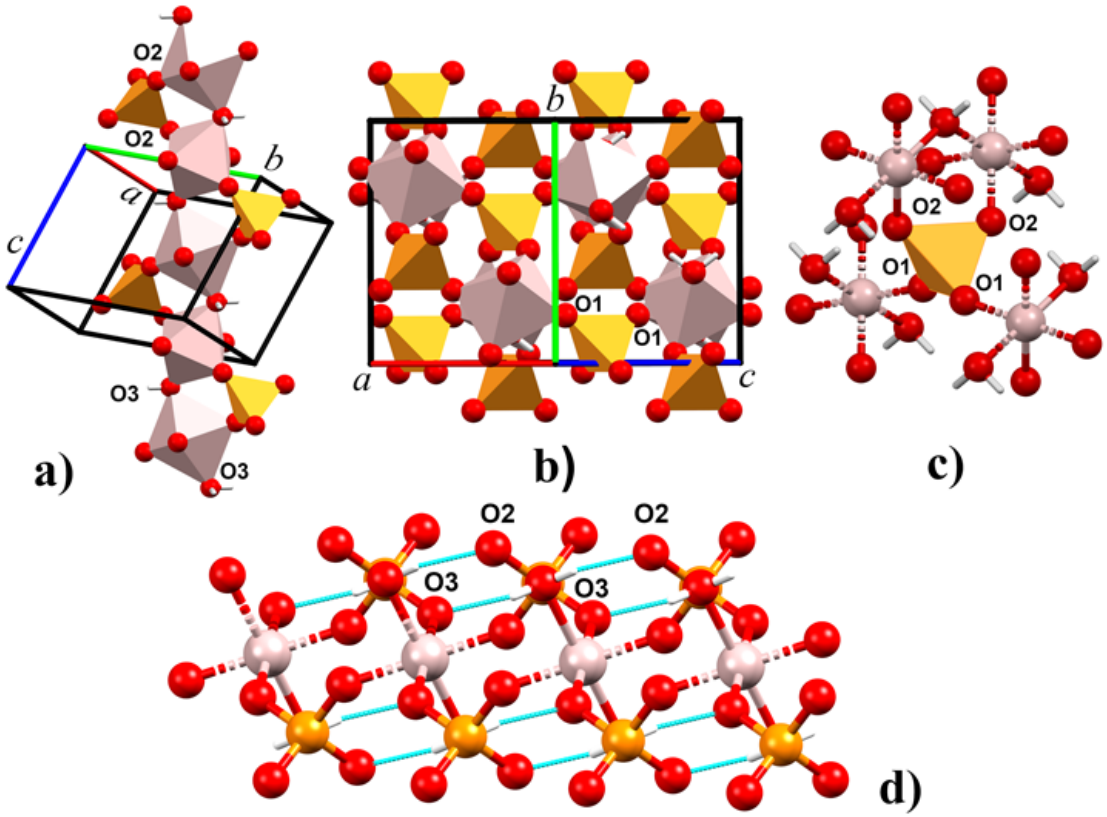

Fig. 4. Structure of ermeloite: (a) corner-sharing (AlO_6)-octahedral chain along [101] direction; (b) mixed tetrahedral- octahedral (PO_4-AlO_6) framework; (c) cation octahedral detail; (d) H-bond interactions.

https://doi.org/10.1180/mgm.2024.33 Published online by Cambridge University Press

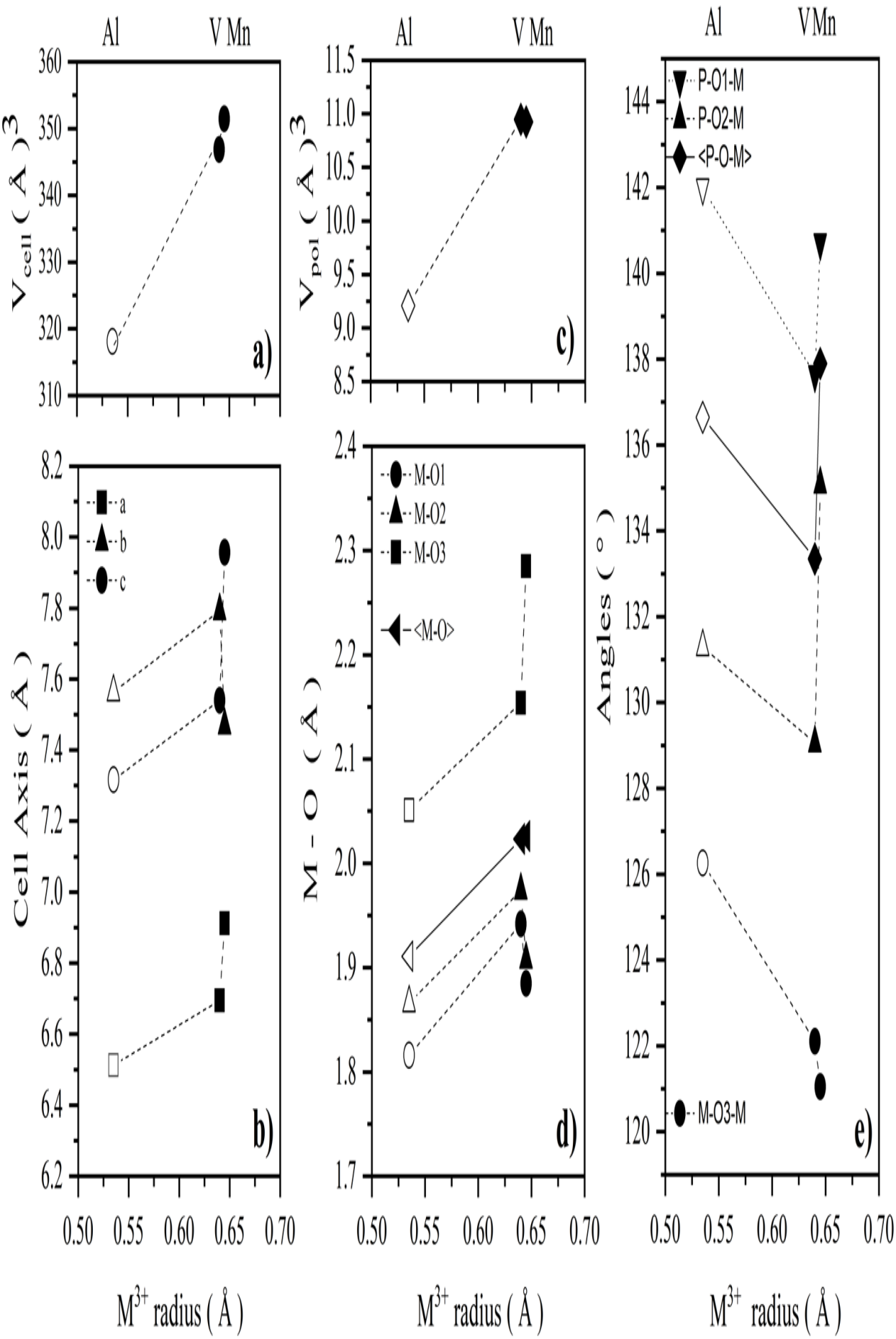

https://doi.org/10.1180/mgm.2024.33 Published online by Cambridge University Press

Fig. 5. Influence of cation ionic radius on the cell and structural parameters for ermeloite and isostructural phosphates, a) cell volume, b) cell axis, c) polyhedral volume, d) bond lengths, e) P-O-M and M-O3-M angles. Ermeloite (open dot)

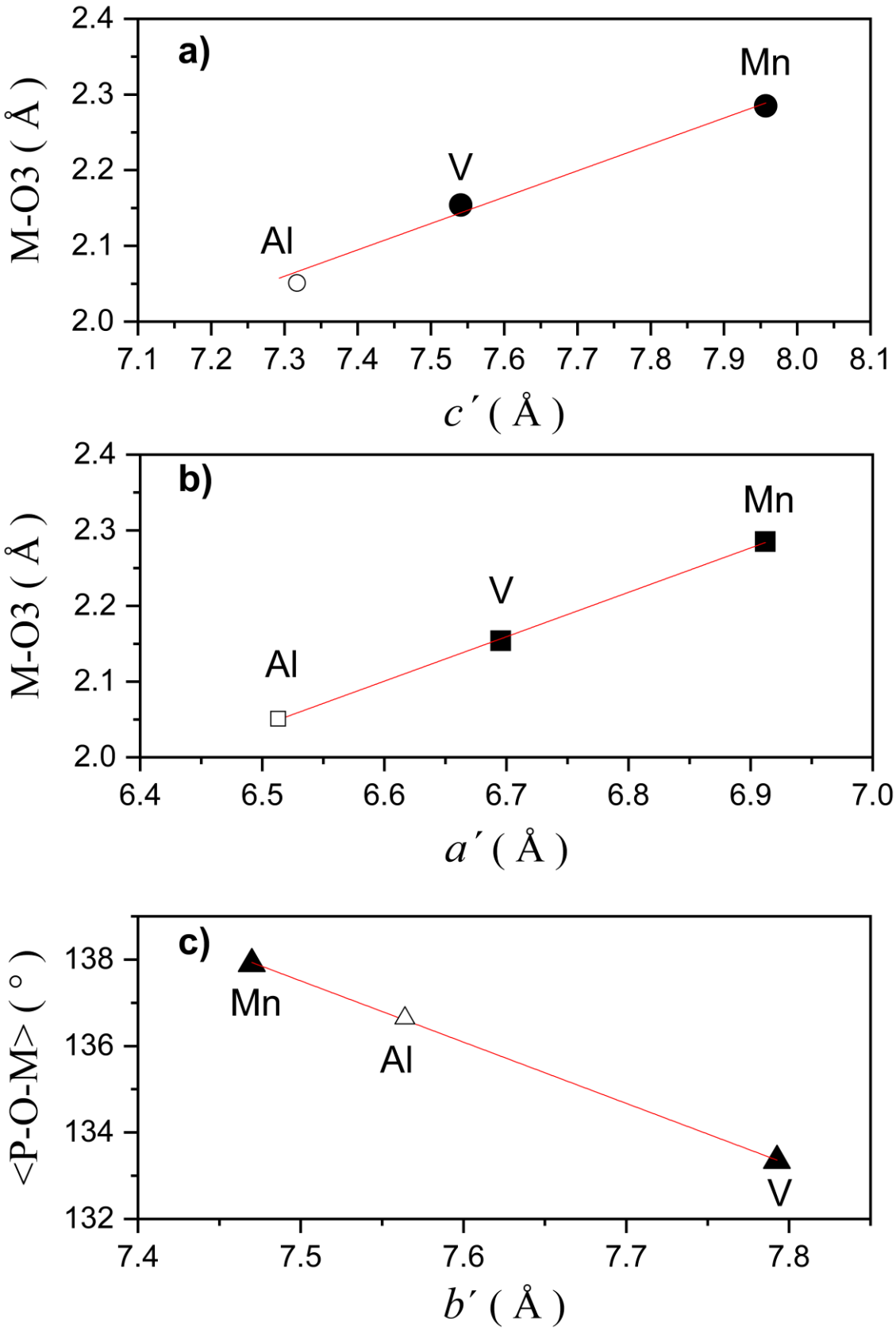

Fig. 6. Relationship between cell axis lengths and geometric parameters for ermeloite

https://doi.org/10.1180/mgm.2024.33 Published online by Cambridge University Press

and isostructural phosphates, a) *c´* axis Vs M-O3 bonds, b) *a´* axis Vs M-O3 bonds, c) average P-O-M angle Vs *b´*. Ermeloite (open dot)

List of tables

Table 1. X-ray powder diffraction data (*d* in Å) for ermeloite. (8 strongest lines in bold). Calculated unit cell parameters: monoclinic *C2/c* with *a* = 6,5393 (32), *b* = 7,5716 (32), *c* = 7,1200 (34) Å, *β* = 115.337(1)°. *R p*= 8.91, *R wp* = 11.57, *R exp* = 10.97, *GOF* = 1.05.

Iobs	*Icalc*	*dmeas*	*dcalc*	*hkl*
76,56	**67,68**	**4,6611**	**4,6588**	**1 1 0**
40,54	**44,15**	**4,5800**	**4,5779**	**1 1 -1**
100,00	**100,00**	**3,2850**	**3,2839**	**1 1 1**
80,02	**74,45**	**3,2640**	**3,2629**	**0 2 1**
49,44	**53,51**	**3,2010**	**3,1999**	**1 1 -2**
15,88	18,10	2,9560	2,9551	2 0 0
34,79	**34,90**	**2,8745**	**2,8737**	**2 0 -2**
39,55	**38,64**	**2,4742**	**2,4736**	**2 2 -1**
33,42	**34,62**	2,4522	2,4516	0 2 -2
14,96	14,36	2,3088	2,3083	1 1 2
11,55	11,21	2,2894	2,2889	2 2 -2
11,29	12,79	2,0753	2,0749	1 3 1
19,48	18,71	2,0560	2,0555	3 1 -2
19,14	19,98	2,0536	2,0532	1 3 -2
25,79	24,48	1,9867	1,9863	2 2 1
9,52	10,09	1,8666	1,8662	0 2 3
14,65	12,10	1,8576	1,8573	3 1 -3
12,36	10,84	1,8226	1,8223	2 0 2
11,55	10,10	1,7386	1,7383	1 1 3
9,05	9,70	1,6414	1,6411	3 3 -1
13,48	12,46	1,6317	1,6315	0 4 2
15,26	14,85	1,6002	1,6000	2 2 -4
19,14	16,44	1,5986	1,5983	3 1 -4
17,80	17,73	1,5941	1,5939	2 4 0
14,65	14,32	1,5262	1,5259	3 3 -3
13,48	12,18	1,4581	1,4579	1 3 3

Table 2. Single crystal experimental details for ermeloite. Crystal data.

Ideal formula	$AlPO_4 \cdot H_2O$

https://doi.org/10.1180/mgm.2024.33 Published online by Cambridge University Press

Crystal dimensions (mm)	0.05 × 0.04 × 0.03
Crystal system, Space group	Monoclinic, *C*2/*c*
Temperature (K)	298(2)
a, b, c (Å)	6.5371(4), 7.5670(5), 7.1146(5)
β (°)	115.335(2)
V (Å^3)	318.08(4)
Z	4
Calculated density (g cm^{-3})	2.92
μ (mm^{-1})	1.009
Data Collection	
Crystal description	Prismatic, transparent, light blue
Instrument	Bruker D8 Venture Photon III 14
Radiation type, wavelength (Å)	MoK*α,* 0.71073
Θ range (˚)	4.38 to 28.29
Absorption correction	multi-scan Bruker Sadabs-2016/2
T_{min}, T_{max}	0.873, 0.959
No. of measured, independent and observed [I>2σ] reflections	3116, 397, 367
R_{int}	0.031
Data completeness to 30.5ºθ (%)	100
Indices range of h, k, l	-7 ≤ h ≤ 8, -10 ≤ k ≤ 10, -9 ≤ l ≤ 9
Refinement	
Refinement method	Full-matrix least squares on F^2
Number of reflections, parameters, restraints	397, 39, 0
$R_1[I > 2\sigma(I)]$, R_1 (all)	0.0209, 0.0235
wR_2 $[I > 2\sigma(I)]$, wR_2 (all)	0.0503, 0.0513
GoF	1.21
No. of refined parameters	39
$\Delta\rho_{max}$ (eÅ^{-3})/$\Delta\rho_{min}$ (eÅ^{-3})	0.32/-0.4

$R_{int} = \Sigma|F_o^2 - F_o^2\ (mean)|/\Sigma[F_o^2]$. $GoF = S = \{\Sigma[w(F_o^2 - F_c^2)^2]/(n-p)\}^{½}$. $R_1 = \Sigma||F_o|-|F_c|| / \Sigma|F_o|$. $wR_2 = \{\Sigma[w(F_o^2 - F_c^2)^2]/\Sigma[w(F_o^2)^2]\}^{½}$; $w = 1/[\sigma^2(F_o^2)+(aP)^2+bP]$ where a is 0.0057, b is 1.0188 and P is $[F_o^2+2F_c^2]/3$.

Table 3. Compositional data for ermeloite expressed as oxides wt%. *by diference. Jarosewich, et al. (1980)[1]. McGuire et al. (1992)[2]..Number of representative analyses: 18

Constituent	Mean	Range	S.D (σ)	Probe standard
Al_2O_3	37.360	38.591-36.284	0.633	Albite[2]
FeO	0.079	0.136-0.042	0.027	Almandine[1]
K_2O	0.108	0.157-0.048	0.035	Microcline[1]
P_2O_5	48.330	49.153-47.622	0.442	Fluorapatite[1]
F	0.755	0.981-0.576	0.117	Fluorapatite[1]
F≡O	-0.318	-0.242/-0.413	0.049	-
H_2O (*)	13.69	15.314-11.561	1.014	-

https://doi.org/10.1180/mgm.2024.33 Published online by Cambridge University Press

Total	100%

Table 4. Atomic coordinates and displacement parametes.

Si	*x*/*a*	*y*/*b*	*z*/*c*	U_{eq}	U^{11}	U^{22}	U^{33}	U^{23}	U^{13}	U^{12}
Al	1⁄4	3⁄4	1⁄2	0.010	0.012	0.009	0.012	0.000	0.006	0.001
P	1⁄2	0.58251	1⁄4	0.009	0.009	0.008	0.010	0	0.005	0
O	0.461	0.69597	0.407	0.011	0.012	0.011	0.013	-	0.007	-
O	0.289	0.46405	0.141	0.012	0.011	0.010	0.014	-	0.006	-
O	0	0.6275(	1⁄4	0.012	0.011	0.014	0.011	0	0.006	0
H	-	0.559(4)	0.293(	0.043(	-	-	-	-	-	-

Table 5. Selected interatomic distances and angles for [$AlPO_4 \cdot H_2O$]. [a] plus 2× corresponding obtuse angles. Symmetry codes: (i) *x*,*y*,*z*; (ii) *x*−1/2, −*y*+1/2, *z*−1/2; (iii) −*x*+1/2, *y*+1/2, −*z*+1/2; (iv) −*x*, −*y*+1, −*z*; (v) −*x*, *y*, −*z*+1/2; (vi) −*x*+1/2, *y*−1/2, −*z*+1/2.

Al-O(1)$^{ii, iii}$ (×2)	1.8158(13)	O(1)^{ii} -Al-O(1)^{iii}	180
Al-O(2)$^{i, iii}$ (×2)	1.8662(13)	O(2)^{i} -Al-O(2)^{iv}	180
Al-O(3)$^{i, iii}$ (×2)	2.0509(9)	O(3)^{iv} -Al-O(3)	180
<Al-O>	**1.9110**		
		O(1)^{iii,ii}-Al-O(2)^{i,iv} (×2)[a]	87.13(6)
P-O(1)$^{i, v}$ (×2)	1.5152(14)	O(1)^{iii,iiv}-Al-O(3)^{iv,} (×2)[a]	88.13(4)
P-O(2)$^{i, v}$ (×2)	1.5454(14)	O(2)^{i,iv}-Al-O(3)^{iv,i} (×2)[a]	87.14(6)
<P-O>	**1.5303**	**<O-Al-O>**	**90**
O(2)-P-O(2)^{v}	109.09(11)	Al-O(3)-Al^{v}	126.25(10)
O(1)^{i,v}-P-O(2)^{i,v} (×2)	107.72(7)		
O(1)^{i,v}-P-O(2)^{v,i} (×2)	110.67(7)	O3-H	0.84(3)
O(1)-P-O(1)	110.97(11)	H-O3-H	104(4)
<O-P-O>	**109.47**	O3-H .... O2^{v}	2.6356(17)

Table 6. Bond-valence analysis (v.u.) for ermeloite. * Bond valence analysis was made with lastest values of bond valence parameters included in "bvparm2020.cif" data set from IUCr, following the methodology of (Witzke et al. 2000; Brown 2006).

	Al	P	H	Σ

https://doi.org/10.1180/mgm.2024.33 Published online by Cambridge University Press

O(1)	0.640 $^{\times 2\downarrow}$	1.317 $^{\times 2\downarrow}$		1.957
O(2)	0.559 $^{\times 2\downarrow}$	1.214 $^{\times 2\downarrow}$	0.255	2.028
O(3)	0.339 $^{\times 2\downarrow\rightarrow}$		0.745 $^{\times 2\rightarrow}$	2.168
Σ	3.077	5.062	1	

https://doi.org/10.1180/mgm.2024.33 Published online by Cambridge University Press